nature genetics

A cascade of arabinosyltransferases controls shoot meristem size in tomato

Cao Xu[1,9], Katie L Liberatore[1,2,8,9], Cora A MacAlister[1,8], Zejun Huang[3,8], Yi-Hsuan Chu[3], Ke Jiang[1,8], Christopher Brooks[1], Mari Ogawa-Ohnishi[4], Guangyan Xiong[5,8], Markus Pauly[5,6], Joyce Van Eck[7], Yoshikatsu Matsubayashi[4], Esther van der Knaap[3] & Zachary B Lippman[1,2]

Shoot meristems of plants are composed of stem cells that are continuously replenished through a classical feedback circuit involving the homeobox *WUSCHEL* (*WUS*) gene and the *CLAVATA* (*CLV*) gene signaling pathway. In CLV signaling, the CLV1 receptor complex is bound by CLV3, a secreted peptide modified with sugars. However, the pathway responsible for modifying CLV3 and its relevance for CLV signaling are unknown. Here we show that tomato inflorescence branching mutants with extra flower and fruit organs due to enlarged meristems are defective in arabinosyltransferase genes. The most extreme mutant is disrupted in a hydroxyproline O-arabinosyltransferase and can be rescued with arabinosylated CLV3. Weaker mutants are defective in arabinosyltransferases that extend arabinose chains, indicating that CLV3 must be fully arabinosylated to maintain meristem size. Finally, we show that a mutation in *CLV3* increased fruit size during domestication. Our findings uncover a new layer of complexity in the control of plant stem cell proliferation.

A wide range of inflorescence architectures exist among closely related plants[1], and this variation can be explained in part by the rate at which meristems terminate in flowers and initiate new branch meristems from which new flowers will form[2,3]. However, less appreciated is the role of meristem size in shoot architecture, as well as in flower and fruit production. In maize, for example, variation in meristem size can account for differences in kernel row number between inbred lines[4], and high row number is a major driver of yield in cultivated hybrids[5]. Meristem size is controlled by a maintenance mechanism that replenishes stem cells lost to lateral organ formation[6]. In *Arabidopsis thaliana*, meristem maintenance is based on a feedback system comprising the stem cell–promoting WUS homeodomain transcription factor and CLV signaling proteins. CLV signaling involves binding of the glycopeptide CLV3 to cell surface leucine-rich repeat (LRR) receptor complexes that include the receptor kinase CLV1 and related LRR receptors[7–10]. These interactions initiate a signaling cascade that restricts *WUS* expression to prevent stem cell overproliferation, and, through negative feedback, WUS promotes *CLV3* expression to limit its own activity[11]. Mutations in *CLV* pathway genes cause meristems to enlarge, which can lead to increased shoot and inflorescence branching, more flowers, and extra organs in flowers and fruits. Studies on mutants with these phenotypes in maize and rice have shown that the *CLV* pathway is conserved in dicots and monocots[12]. However, little is known about the genes and molecular mechanisms underlying stem cell proliferation in other crops, leaving unanswered whether the *CLV* pathway or other pathways are important in controlling meristem size and productivity. Here we investigate the control of meristem size in tomato.

RESULTS

Tomato *fab* and *fin* mutants have enlarged meristems

We explored the genetic control of inflorescence architecture in tomato by screening a large ethyl methanesulfonate (EMS) and fast neutron (FN) mutagenesis population for mutants with increased inflorescence branching[13]. In contrast to previously characterized mutants in which unbranched wild-type inflorescences are transformed into highly branched structures with normal flowers as a result of delay in meristem maturation[3,14], we identified six new mutants where branching was associated with fasciated flowers having more floral organs than wild-type flowers (**Fig. 1a–h**). Complementation tests identified two loci that we designated *fasciated and branched* (*fab*: one EMS allele) and *fasciated inflorescence* (*fin*: two EMS and three FN alleles).

[1]Cold Spring Harbor Laboratory, Cold Spring Harbor, New York, USA. [2]Watson School of Biological Sciences, Cold Spring Harbor Laboratory, Cold Spring Harbor, New York, USA. [3]Department of Horticulture and Crop Science, Ohio State University, Wooster, Ohio, USA. [4]Division of Biological Science, Graduate School of Science, Nagoya University, Chikusa, Nagoya, Japan. [5]Energy Biosciences Institute, University of California, Berkeley, Berkeley, California, USA. [6]Department of Plant and Microbial Biology, University of California, Berkeley, Berkeley, California, USA. [7]Boyce Thompson Institute for Plant Science, Ithaca, New York, USA. [8]Present addresses: Cereal Disease Laboratory, US Department of Agriculture, Agriculture Research Service, St. Paul, Minnesota, USA (K.L.L.), Department of Molecular, Cellular and Developmental Biology, University of Michigan, Ann Arbor, Michigan, USA (C.A.M.), Chinese Academy of Agricultural Sciences, Institute of Vegetables and Flowers, Beijing, China (Z.H.), Dow AgroSciences, LLC, Indianapolis, Indiana, USA (K.J.) and Department of Anatomical Sciences and Neurobiology, University of Louisville, Louisville, Kentucky, USA (G.X.). [9]These authors contributed equally to this work. Correspondence should be addressed to Z.B.L. (lippman@cshl.edu).

Received 22 February; accepted 27 April; published online 25 May 2015; doi:10.1038/ng.3309

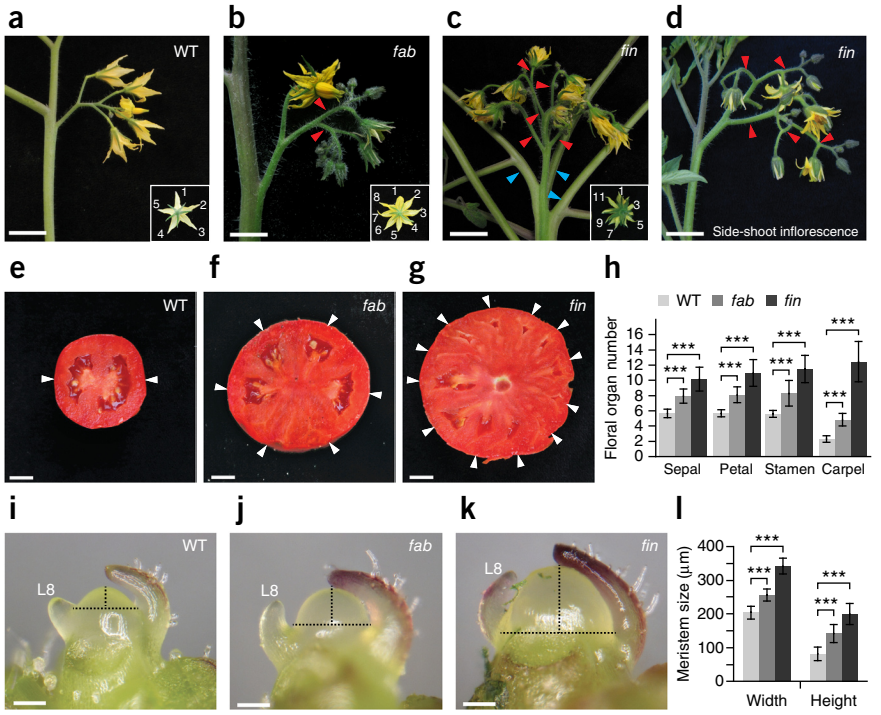

Figure 1 The *fab* and *fin* mutants develop branched inflorescences with fasciated flowers as a consequence of enlarged meristems. (**a**) An unbranched inflorescence typical of a wild-type (WT) plant and a typical wild-type flower (inset). (**b**,**c**) Primary inflorescences from *fab* (**b**) and *fin* (**c**) mutants showing branching and fasciated flowers (insets). (**d**) A branched inflorescence from a *fin* side shoot. Red arrowheads, branches; blue arrowheads, extra side shoots. (**e**–**g**) Wild-type fruits produce two locules (**e**), whereas the fruits of *fab* (**f**) and *fin* (**g**) mutants develop extra locules. Arrowheads, locules. (**h**) Quantification and comparison of floral organ numbers in wild-type, *fab* and *fin* flowers. (**i**–**k**) Stereoscope images of the primary SAM from wild-type (**i**), *fab* (**j**) and *fin* (**k**) plants at the transition meristem (TM) stage, before formation of the first flower. Dashed lines mark the width and height used to measure meristem size. L8, leaf 8. (**l**) Quantification of TM size from wild-type, *fab* and *fin* plants. Data are means ± s.d.; $n = 25$ (**h**) and 9–13 (**l**). A two-tailed, two-sample *t* test was performed, and significant differences are represented by black asterisks: $***P < 0.0001$. Scale bars: 1 cm (**a**–**g**) and 100 µm (**i**–**k**).

Inflorescence branching in *fin* mutants was more severe than in *fab* mutants, and *fin* plants also developed a highly fasciated primary shoot with more side shoots than wild-type plants (**Fig. 1a–d**). Both mutants produced larger fruits as a consequence of additional carpels, with *fin* mutants bearing the largest fruits (**Fig. 1e–g**). We designated a strong allele of *fin* as a reference (*fin-e4489*, hereafter *fin* unless otherwise noted), and quantification of floral organs in the corresponding plants confirmed greater fasciation than in *fab* plants (**Fig. 1h**). Analyses of double mutants of *fab* and *fin* with the meristem maturation mutants *compound inflorescence* (*s*) and *anantha* (*an*), defective in the homolog of *Arabidopsis WUSCHEL-RELATED HOMEOBOX 9* and the floral-identity gene *UNUSUAL FLORAL ORGANS*, respectively, showed additive genetic relationships, indicating that the genes underlying *fin* and *fab* act separately from the meristem maturation pathway (**Supplementary Fig. 1**)[14].

The phenotypes of *fab* and *fin* mutants were reminiscent of *CLV* gene mutants in *Arabidopsis*, in which inflorescence and flower fasciation are caused by enlarged shoot apical meristems (SAMs)[7,8,10,15]. The vegetative SAMs of the *fab* and *fin* mutants, unlike those of the *s* and *an* mutants[14], were larger than wild-type SAMs (**Supplementary Fig. 2a–d**), and this effect became more pronounced at the reproductive transition stage, just before formation of the first flower (**Fig. 1i–l**). We investigated meristem development in *fin* mutants using scanning electron microscopy (SEM) and found that the enlarged SAM allowed more leaf primordia and thus axillary branch meristems to develop (**Supplementary Fig. 2e–l**).

The phenotypic similarities between the *fab* and *fin* mutants and the fact that *fab* and *fin* double-mutant plants were more fasciated than either single mutant alone (**Supplementary Fig. 3**) suggested a functional link in controlling meristem size. To better understand the relationship between these mutants, we compared RNA sequencing profiles from *fab*, *fin* and wild-type vegetative primary shoot apices (Online Methods). We detected a 2-fold or greater difference in expression for 679 genes in *fab* mutants and 1,194 genes in *fin* mutants in comparison to wild-type apices (Online Methods and **Supplementary Table 1**). Notably, there was significant overlap ($P < 0.001$) among the differentially expressed genes (**Fig. 2a**), suggesting that the *FAB* and *FIN* genes could act in the same pathway. Because *fab* and *fin* meristems were enlarged, we checked for expression changes in the homolog of *WUS* (*SlWUS*, *Solyc02g083950*)[16,17] and a likely functional homolog of *CLV3* (*SlCLV3*, *Solyc11g071380*) (**Supplementary Fig. 4a–c**)[18]. Despite a 25-fold increase in *SlCLV3* expression, *SlWUS* expression doubled in *fin* meristems (**Fig. 2b** and **Supplementary Table 1**). CLV-WUS feedback was also mildly affected in *fab* mutants: *SlCLV3* expression was upregulated by nearly fivefold, but *SlWUS* expression was maintained, consistent with a minor increase in vegetative meristem size (**Supplementary Fig. 2a–d** and **Supplementary Table 1**). Notably, two additional CLV3/EMBRYO-SURROUNDING REGION (CLE) genes (*SlCLE3*, *Solyc02g067550*; *SlCLE9*, *Solyc06g074060*) were also upregulated in *fin* mutants (**Fig. 2b** and **Supplementary Fig. 4d,e**)[18]. We validated the expression changes for *SlWUS* and *SlCLV3* using *in situ* hybridization, which further showed substantial expansion of their expression domains in *fin* meristems, consistent with stem cell overproliferation (**Fig. 2c**).

FAB encodes CLV1, and *FIN* encodes an arabinosyltransferase

We used a mapping strategy to clone the genomic regions underlying the *fab* and *fin* mutants, using F_2 populations derived from crosses with the wild tomato *Solanum pimpinellifolium* (**Fig. 2d,e** and Online Methods). *fab* mapped to a 325-kb interval on the south arm of chromosome 4 where the closest homolog of *CLV1* (*Solyc04g081590*) is located (**Fig. 2d** and **Supplementary Fig. 5a**). Like *CLV1* (ref. 7), *Solyc04g081590* was expressed in all tissue types, including meristems, and sequencing its coding region in the *fab* mutant identified a missense mutation affecting the kinase domain (**Fig. 2d,f** and **Supplementary Fig. 5b**). Notably, the classical, weakly dominant-negative *clv1-9* allele encodes the same amino acid change[19], and plants heterozygous for the *fab* mutation exhibited weak fasciation (**Supplementary Fig. 6**).

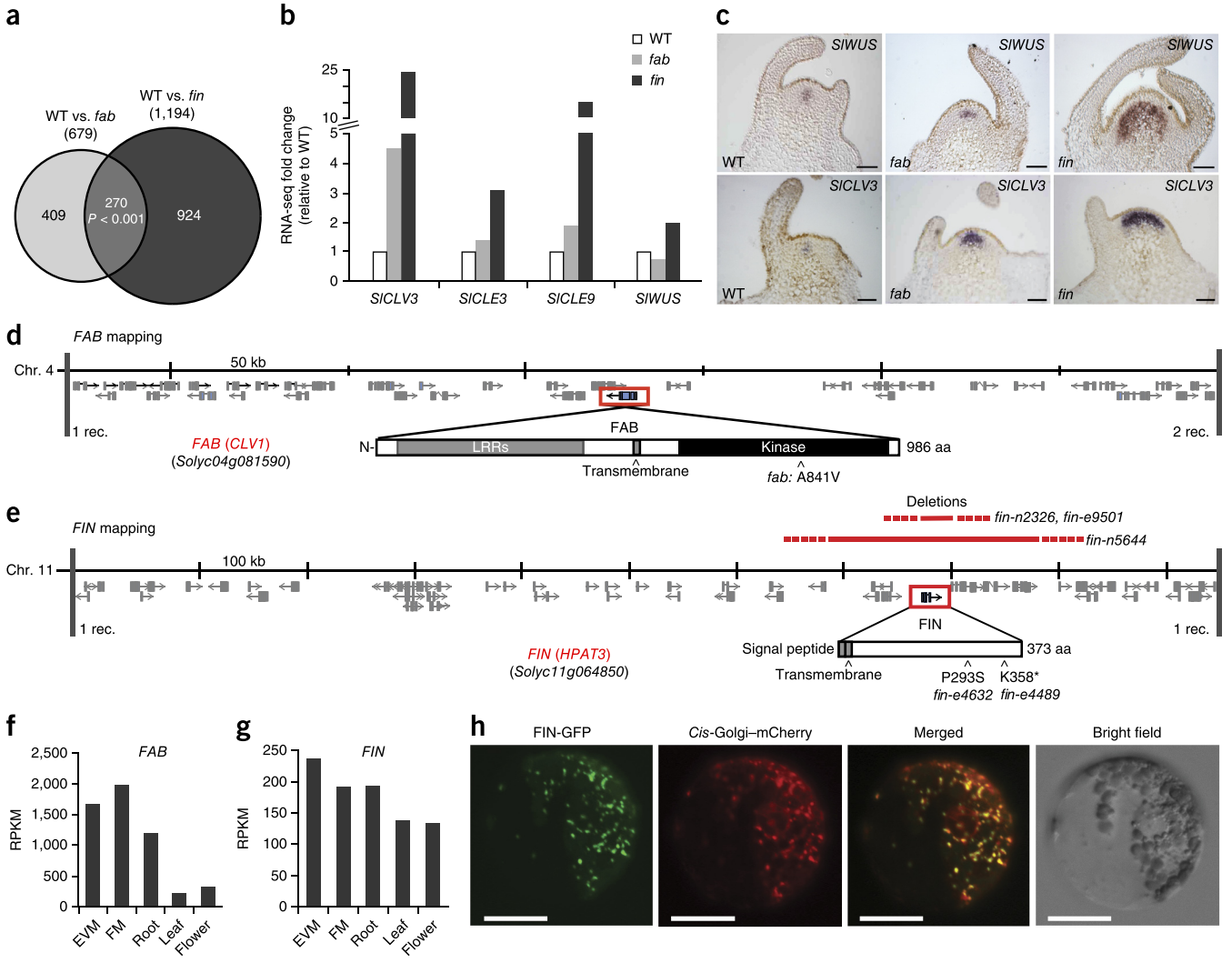

Figure 2 Molecular characterization and positional cloning of the *fin* and *fab* mutants. (**a**) Venn diagram showing significant overlap of differentially expressed genes ($P < 0.001$) in wild-type versus *fab* (light gray) and wild-type versus *fin* (dark gray) vegetative apices by RNA sequencing. (**b**) Fold change in expression of *SlCLV3*, *SlCLE3*, *SlCLE9* and *SlWUS* in *fin* and *fab* vegetative apices relative to wild-type apices by RNA sequencing (RNA-seq). (**c**) mRNA *in situ* hybridization showing substantial expansion in *fin* (right) and mild expansion in *fab* (center) of the *SlWUS* and *SlCLV3* expression domains in vegetative meristems in comparison to wild type (left). (**d**,**e**) The mapping intervals for *FAB* (**d**) and *FIN* (**e**). The *FAB* and *FIN* genes are boxed in red. Protein diagrams are shown with characteristic domains and motifs labeled. Open arrows indicate point mutations and corresponding amino acid changes from *fab-e0497* and two alleles of *fin*. Red horizontal lines in **e** represent three *fin* deletion alleles, which do not produce transcripts (**Supplementary Fig. 5d**). Rec., recombinant. (**f**,**g**) RNA sequencing read counts (RPKM) for *FAB* (**f**) and *FIN* (**g**) in major tissues, including the early vegetative meristem (EVM) and floral meristem (FM). (**h**) Subcellular colocalization of the transiently expressed FIN-GFP fusion protein with a *cis*-Golgi marker (Man49) in tomato protoplasts (Online Methods). Scale bars: 100 µm (**c**) and 10 µm (**h**).

fin mapped to a 1.1-Mb region in the middle of chromosome 11 containing 71 genes. RNA sequencing identified a nonsense mutation in *Solyc11g064850*, encoding a homolog of the recently identified hydroxyproline O-arabinosyltransferase (HPAT) protein family in *Arabidopsis* (**Fig. 2e** and **Supplementary Fig. 5c**)[20]. Sanger sequencing of *Solyc11g064850* from four additional *fin* alleles found a missense mutation and deletions (**Fig. 2e**). RT-PCR confirmed that *Solyc11g064850* transcripts were absent in plants with the deletion alleles (**Supplementary Fig. 5d**). Thus, *FAB* encodes the tomato homolog of CLV1, and *FIN* encodes a predicted HPAT protein.

HPATs are Golgi-localized type II transmembrane proteins that are structurally similar to members of the GT8 glycosyltransferase family and catalyze the transfer of L-arabinose to the hydroxyl group of hydroxyproline (Hyp) residues[20]. Hyp O-arabinosylation is primarily found in the form of linear oligoarabinoside chains on extracellular Hyp-rich glycoproteins (HRGPs), such as cell wall–associated extensins[21–23]. There are three *HPAT* genes in *Arabidopsis*, and extensins are underarabinosylated in *hpat3* mutants and in *hpat1* and *hpat2* double mutants[20]. Although cell wall thickness is reduced in *hpat1* and *hpat2* double-mutant plants, perhaps accounting for a range of pleiotropic growth defects, none of the available *HPAT* gene mutants show defects in meristem size[20].

FIN is one of four *HPAT* gene homologs in tomato and is most similar to *HPAT3* (**Supplementary Fig. 5c**). *FIN* is expressed in all tissue types (**Fig. 2g**), and transiently expressed FIN-GFP fusion proteins in tomato protoplasts colocalized with a Golgi marker (**Fig. 2h**). To determine whether altered extensin arabinosylation might explain *fin* mutant phenotypes, we measured the monosaccharide composition

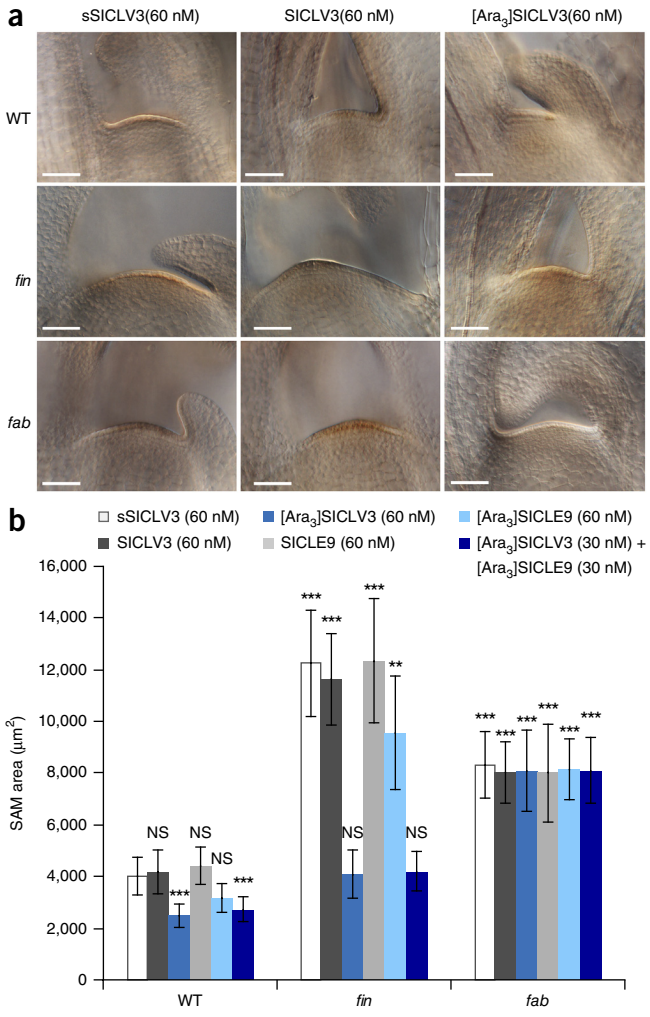

Figure 3 Arabinosylated SICLE peptides rescue *fin* meristem enlargement. (**a**) Representative images showing the SAMs of wild-type (top), *fin* (middle) and *fab* (bottom) plants treated with 60 nM of different versions of synthetic SICLV3 peptide. Triarabinosylated SICLV3 ([Ara_3]SICLV3) rescues the enlarged SAM of *fin* mutants, reducing it to a size comparable to that of wild-type SAMs. sSICLV3, scrambled SICLV3; SICLV3, SICLV3 peptide devoid of arabinosylation. Scale bars, 100 µm. (**b**) Quantification of wild-type, *fin* and *fab* SAM sizes after treatment with different versions of SICLV3 and SICLE9 peptides. The area of each SAM was captured and measured with ImageJ software (Online Methods). Data are presented as means ± s.d.; $n = 30–46$. All treatments were compared in a pairwise manner to the common control of wild type treated with scrambled SICLV3 (Dunnett's 'compare with control', $^{***}P < 0.0001$, $^{**}P < 0.001$; NS, not significant).

of cell wall components isolated from the shoot apices of *fin*, *fab* and wild-type plants (Online Methods). We found no differences in arabinose content in extensin fractions (**Supplementary Table 2**). Moreover, transmission electron microscopy did not identify differences in cell wall thickness among *fin*, *fab* and wild-type meristems (**Supplementary Fig. 7**). Thus, meristem enlargement in *fin* mutants is not a result of changes in extensin arabinosylation or related cell wall defects.

Engineered mutants of the tomato *CLV* pathway are fasciated

Hyp O-arabinosylation is also found on secreted signaling peptides[24], including the CLE peptide family[9]. CLE peptides are proteolytically processed from the C termini of pre-propeptides[25]. The mature form of CLV3 is a 12- or 13-residue glycopeptide modified with three L-arabinose residues on a Hyp residue at position 7 (Hyp7)[9,26]. Molecular modeling suggests that the triarabinoside chain induces conformational changes that have important effects on binding and specificity for receptor proteins[26]. In support of this hypothesis, chemically synthesized triarabinosylated CLV3 ([Ara_3]CLV3) interacts *in vitro* with CLV1 more strongly than unmodified CLV3 (ref. 9) and can rescue the enlarged meristems of *clv3* mutants more effectively when applied exogenously[26].

We tested whether SlCLV3 peptide controls meristem size in tomato by engineering null mutations in *SlCLV3* using CRISPR/Cas9 gene-editing technology[27–29]. Using a CRISPR/Cas9 construct containing two single-guide RNAs (sgRNAs)[29], we generated four first-generation (T_0) transgenic CRISPR (*CR*)-*slclv3* plants that developed branched inflorescences with fasciated flowers, closely resembling *fin* mutants (Online Methods and **Supplementary Fig. 8a–d**). PCR genotyping and sequencing identified insertions and deletions (indels) in proximity to both sgRNA target sequences for all alleles (Online Methods and **Supplementary Fig. 8e**). We also engineered mutations in *FAB* and *SlCLV2* (*Solyc04g056640*), a homolog of *Arabidopsis CLV2* encoding an LRR receptor–like protein that acts redundantly with CLV1 (**Supplementary Fig. 5a**)[15,30]. *CR-fab* and *CR-clv2* T_0 plants were weakly fasciated like *fab* mutants (**Supplementary Figs. 9** and **10**). Notably, we validated fasciation for the CRISPR/Cas9 *clv* mutants in T_1 progeny plants (**Supplementary Table 3**). These findings demonstrate that the function of the *clv* meristem maintenance pathway is conserved in tomato.

Arabinosylated SlCLV3 can rescue *fin* mutants

The enlarged meristems of *fin* mutants are in striking contrast to the dramatic upregulation of *SlCLE* genes, suggesting that a defect in CLV signaling may be due to a failure to post-translationally arabinosylate SlCLV3 and/or other CLE peptides. In support of this hypothesis, arabinosylation of *Arabidopsis* CLE2 is reduced when this peptide is overexpressed in *hpat3* mutants but not in *hpat1* and *hpat2* double mutants, suggesting that HPATs are not equally responsible for arabinosylation of all CLE peptides[20]. As *in vitro* modification assays using recombinantly expressed FIN or HPAT3 from yeast and tobacco BY-2 cell lines have been unable to detect arabinosyltransferase activity on synthesized [Hyp7]SlCLV3 or [Hyp7]CLV3 (data not shown and ref. 20), we treated live apices with CLE peptides (Online Methods). If loss of CLE arabinosylation causes *fin* mutant phenotypes, then arabinosylated SlCLE peptides should rescue the enlarged meristems. We synthesized [Ara_3]SlCLV3 and [Ara_3]SlCLE9 and grew seedlings in liquid culture in the presence of a low concentration of each peptide[9,26]. SAMs from *fin* seedlings grown with 60 nM [Ara_3]SlCLV3 or [Ara_3]SlCLE9 were substantially reduced in size (**Fig. 3a,b** and **Supplementary Table 4**). This effect was greater with [Ara_3]SlCLV3, resulting in a meristem size comparable to that of wild-type plants treated with non-arabinosylated or scrambled SlCLV3. Notably, combining 30 nM [Ara_3]SlCLV3 with 30 nM [Ara_3]SlCLE9 resulted in a rescue of *fin* meristem size similar to that observed with 60 nM [Ara_3]SlCLV3, implying a role for SlCLE9 in CLV signaling (**Fig. 3b** and **Supplementary Table 4**). *fab* meristems were insensitive to all [Ara_3]SlCLE treatments, consistent with a defect in transducing CLE peptide signals[25]. These results support the model that stem cell overproliferation in *fin* meristems is due to a break in the CLV-WUS circuit, caused by a failure to form triarabinosylated CLE peptides.

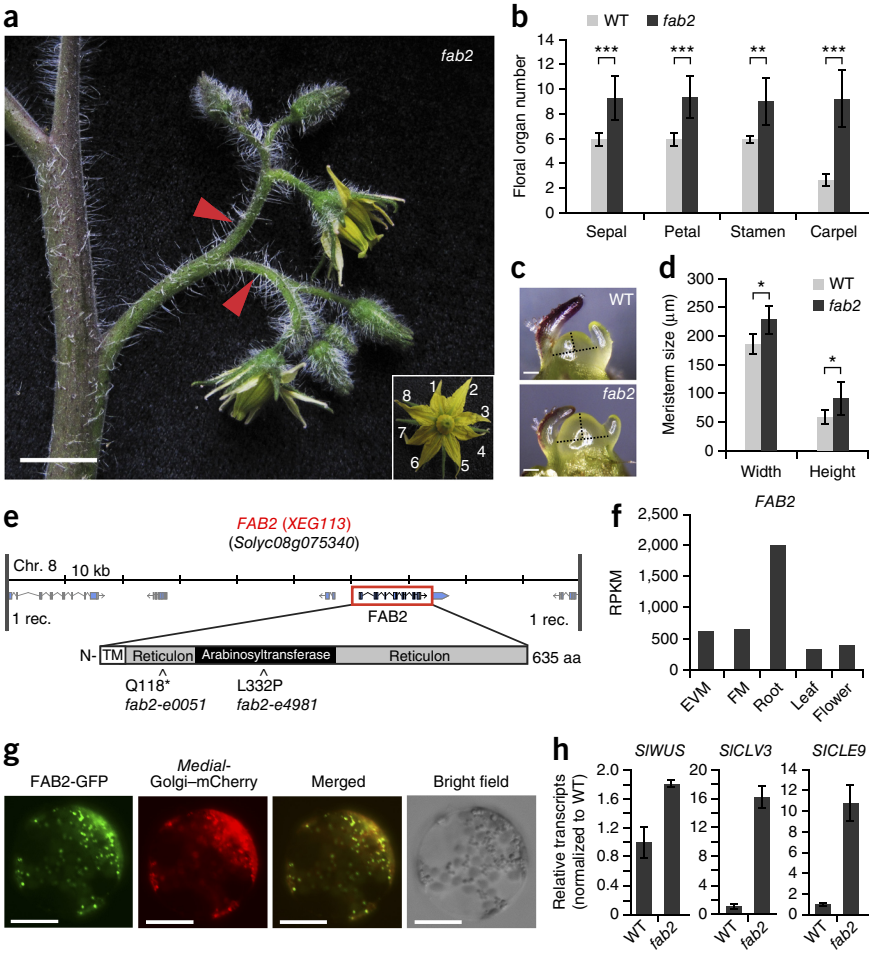

Figure 4 The *fab2* mutant is defective in an arabinosyltransferase gene predicted to extend arabinose chains. (**a**) Primary inflorescence from a *fab2* mutant and a representative flower (inset). Red arrowheads mark branches. (**b**) Quantification and comparison of floral organ numbers in *fab2* and wild-type plants. (**c**) Stereoscope images of the primary SAM of *fab2* plants, showing an enlarged TM stage in comparison to wild type. Dashed lines mark the height and width used for meristem size quantification. (**d**) Quantification and comparison of TM meristem sizes in *fab2* and wild-type plants. (**e**) Positional cloning of *FAB2*. The *FAB2* gene is boxed in red, and a protein diagram is shown below. Open arrows mark the nonsense and missense point mutations from two independently derived alleles of *fab2*. (**f**) RNA sequencing counts (RPKM) of *FAB2* in major tissue types. (**g**) Subcellular colocalization of transiently expressed FAB2-GFP fusion protein with a *medial*-Golgi marker (Mur3) in tomato protoplasts (Online Methods). (**h**) qRT-PCR showing upregulation of *SlWUS*, *SlCLV3* and *SlCLE9* in *fab2* vegetative apices (Online Methods). Data are means ± s.d.; $n = 13$ (**b**), 8 (**d**) and 3 (**h**). A two-tailed, two-sample *t* test was performed, and significant differences are represented by black asterisks: $***P < 0.0001$, $**P < 0.001$, $*P < 0.01$. Scale bars: 1 cm (**a**), 100 µm (**c**) and 10 µm (**g**).

Loss of an arabinosyltransferase cascade causes fasciation

By rescreening the original mutagenesis population[13] and a new EMS-mutagenized population, we identified two alleles for *fab2*, a mildly fasciated and branched mutant that closely resembled *fab* mutants (**Fig. 4a–d**). Positional cloning of *fab2* identified a missense and nonsense mutation in the tomato homolog of *Arabidopsis XYLOGLUCANASE 113* (*XEG113*), encoding a predicted arabinosyltransferase in the GT77 family (**Fig. 4e** and **Supplementary Fig. 11**). *Arabidopsis* plants with mutations in *XEG113* display predominantly unusual diarabinoside chains on extensins, resulting in longer hypocotyls and shorter root hairs[31,32]. In tomato, *FAB2* is expressed in all tissues and localizes to Golgi like *FIN* (**Fig. 4f,g**). Similar to in *fin* mutants, the expression levels of *SlWUS*, *SlCLV3* and *SlCLE9* were all upregulated in *fab2* SAMs, with *SlCLV3* and *SlCLE9* showing greater than tenfold upregulation in their expression (**Fig. 4h**). Thus, *FAB2*, like *FIN*, is a critical regulator of CLV signaling.

Mutations in *Arabidopsis REDUCED RESIDUAL ARABINOSE 3* (*RRA3*), also encoding an arabinosyltransferase in the GT77 family[33], result in shorter root hairs as a consequence of predominantly monoarabinoside chains on extensins[32]. This observation suggested that RRA3 and XEG113 act sequentially after HPATs to extend arabinoside chains[20,32]. To test whether the tomato homolog of RRA3 functions with FIN and FAB2 in tomato CLV signaling, we mutated the closest homolog of *RRA3* (*Solyc04g080080*) using CRISPR/Cas9 (**Fig. 5** and **Supplementary Fig. 12**)[29]. We identified two *RRA* genes in tomato; both were most similar to *RRA3*, but only *Solyc04g080080* (hereafter referred to as *SlRRA3a*) encoded a predicted transmembrane domain (**Fig. 5a**). *SlRRA3a* is expressed in all tissues, and transiently expressed SlRRA3a-GFP fusion proteins in tomato protoplasts colocalized with a Golgi marker (**Fig. 5b,c**). Eight *CR-slrra3a* plants developed branched inflorescences with fasciated flowers, with these phenotypes more severe than those of the *fab2* mutants, and sequencing identified a range of indel mutations for all alleles, including a homozygous small deletion in one plant (**Fig. 5d–h**). Using quantitative RT-PCR (qRT-PCR), we found that *SlWUS*, *SlCLV3* and *SlCLE9* were all upregulated, with *SlCLV3* and *SlCLE9* showing more than 15-fold higher expression than in wild type (**Fig. 5i**). Thus, *FIN*, *RRA3a* and *FAB2* all function in the tomato *CLV* pathway.

A natural *CLV3* mutation was selected during domestication

Our *CLV* pathway mutants reminded us of naturally occurring fasciation responsible for the dramatic increase in tomato fruit size during domestication[34]. Extreme size is based on more carpels, which increases the number of seed compartments (locules). In comparison to the invariant bilocular fruits of wild tomatoes and most small-fruited cultivars, large-fruited varieties can have eight or more locules[34]. A large portion of this variation is due to *locule number* (*lc*) and *fasciated* (*fas*), two classical mutations that have synergistic effects on locule number and thus fruit size when combined[35,36]. The effect in *lc* mutants is weaker than in *fas* mutants and is likely due to a regulatory mutation downstream of *SlWUS*[16], which has been proposed to affect binding of the tomato homolog of AGAMOUS, a transcription factor that downregulates *WUS* in *Arabidopsis* floral meristems[37]. The mutant *fas* phenotype was reported to be caused by loss of expression of a YABBY transcription factor gene[38]. However, the *YABBY* gene (*Solyc11g071810*) is located on chromosome 11 close to *SlCLV3*, and further dissection of the *fas* locus identified a 294-kb

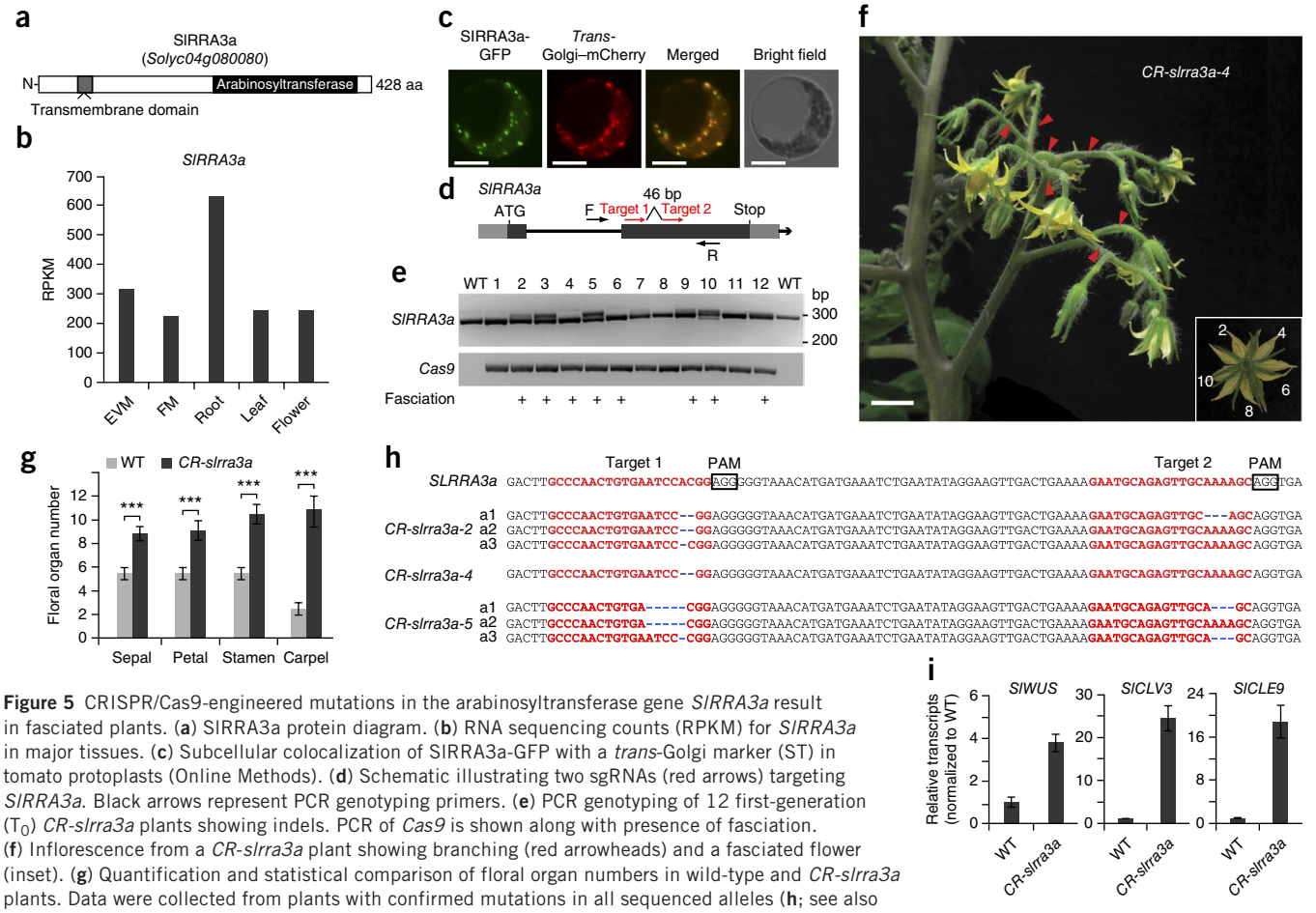

Figure 5 CRISPR/Cas9-engineered mutations in the arabinosyltransferase gene *SlRRA3a* result in fasciated plants. (**a**) SlRRA3a protein diagram. (**b**) RNA sequencing counts (RPKM) for *SlRRA3a* in major tissues. (**c**) Subcellular colocalization of SlRRA3a-GFP with a *trans*-Golgi marker (ST) in tomato protoplasts (Online Methods). (**d**) Schematic illustrating two sgRNAs (red arrows) targeting *SlRRA3a*. Black arrows represent PCR genotyping primers. (**e**) PCR genotyping of 12 first-generation (T_0) *CR-slrra3a* plants showing indels. PCR of *Cas9* is shown along with presence of fasciation. (**f**) Inflorescence from a *CR-slrra3a* plant showing branching (red arrowheads) and a fasciated flower (inset). (**g**) Quantification and statistical comparison of floral organ numbers in wild-type and *CR-slrra3a* plants. Data were collected from plants with confirmed mutations in all sequenced alleles (**h**; see also Online Methods). (**h**) *CR-slrra3a* alleles identified from three T_0 plants. *CR-slrra3a-2* and *CR-slrra3a-5* plants were chimeric, with multiple indels (blue dashed lines and letters). One of each representative allele identified by sequencing is shown. The *CR-slrra3a-4* plant was homozygous for a 2-nt deletion. Red font highlights sgRNA targets, and black boxes indicate protospacer-adjacent motif (PAM) sequences; a, allele. (**i**) qRT-PCR showing upregulation of *SlWUS*, *SlCLV3* and *SlCLE9* in *CR-slrra3a* plants. RNA was extracted from the side-shoot apices of wild-type and *CR-slrra3a* T_0 plants (Online Methods). Data are means ± s.d.; $n = 11$ (**g**) and 3 (**i**). A two-tailed, two-sample *t* test was performed, and significant differences are represented by black asterisks: $^{***}P < 0.0001$. Scale bars: 10 μm (**c**) and 1 cm (**f**).

inversion with breakpoints in intron 1 of *YABBY* and 1 kb upstream of *SlCLV3* (**Fig. 6a**,**b**)[39]. This finding, in combination with weak rescue of the *fas* mutant upon introduction of functional *YABBY*[38], led us to ask whether *SlCLV3* might also contribute to naturally occurring fasciation.

Introgression of the *fas* locus into our standard cultivated background resulted in weak branching and flower and fruit fasciation resembling the phenotype for *CR-clv2* plants (**Fig. 6c** and **Supplementary Fig. 10**). Introgression of *fas* into *S. pimpinellifolium* (*Sp-fas*) produced even weaker fasciation, with little branching and half of all fruits producing three locules, likely owing to the absence of modifier loci in the wild species background[37]. Such a weak effect would be consistent with a change in *SlCLV3* expression[38], and *in situ* hybridization showed reduced expression of *SlCLV3* in the floral meristems of *Sp-fas* plants (**Fig. 6d**). To determine whether *SlCLV3* underlies the *fas* mutant, we carried out transgenic complementation experiments in the *Sp-fas* genotype (Online Methods). We generated 18 plants carrying a construct comprising the *SlCLV3* gene with 5.5 kb of upstream and 3.5 kb of downstream regions (*long-gCLV3*), and all plants were rescued to bilocular, smaller fruits (**Fig. 6e**). In contrast, 16 plants transformed with a similar construct containing 1 kb upstream of *SlCLV3* (up to the inversion breakpoint; *short-gCLV3*) did not show reduced locule number (**Fig. 6f**). Notably, we validated these effects in T_1 *long-gCLV3* progeny plants and found that rescue of the *fas* phenotype cosegregated with the transgene (**Fig. 6f**). We therefore conclude that a weak regulatory mutation in *SlCLV3* underlies the *fas* mutant.

DISCUSSION

By uniting forward genetics with CRISPR/Cas9 technology[27], we exposed arabinosyltransferase genes as critical new components of the *CLV* pathway that are essential to control meristem size. As members of the plant and animal glycosyltransferase superfamily[40–42], several putative arabinosyltransferases have recently been found to function in diverse processes, including pollen tube growth by HPATs[20], root hair elongation by RRAs and XEG113 (ref. 32), and Rhizobia-induced nodulation by FIN homologs in pea and clover[43]. Yet, no meristem phenotypes for any available arabinosyltransferase mutants have been reported. Our findings that arabinosyltransferase genes are critical for stem cell homeostasis suggest that members of different arabinosyltransferase families were coopted to target distinct sets of proteins and signaling peptides in different species and developmental contexts. In support of this hypothesis, unlike the predominant fasciation phenotype of *fin* mutants, we found that *fab2* and *CR-rra3a* plants

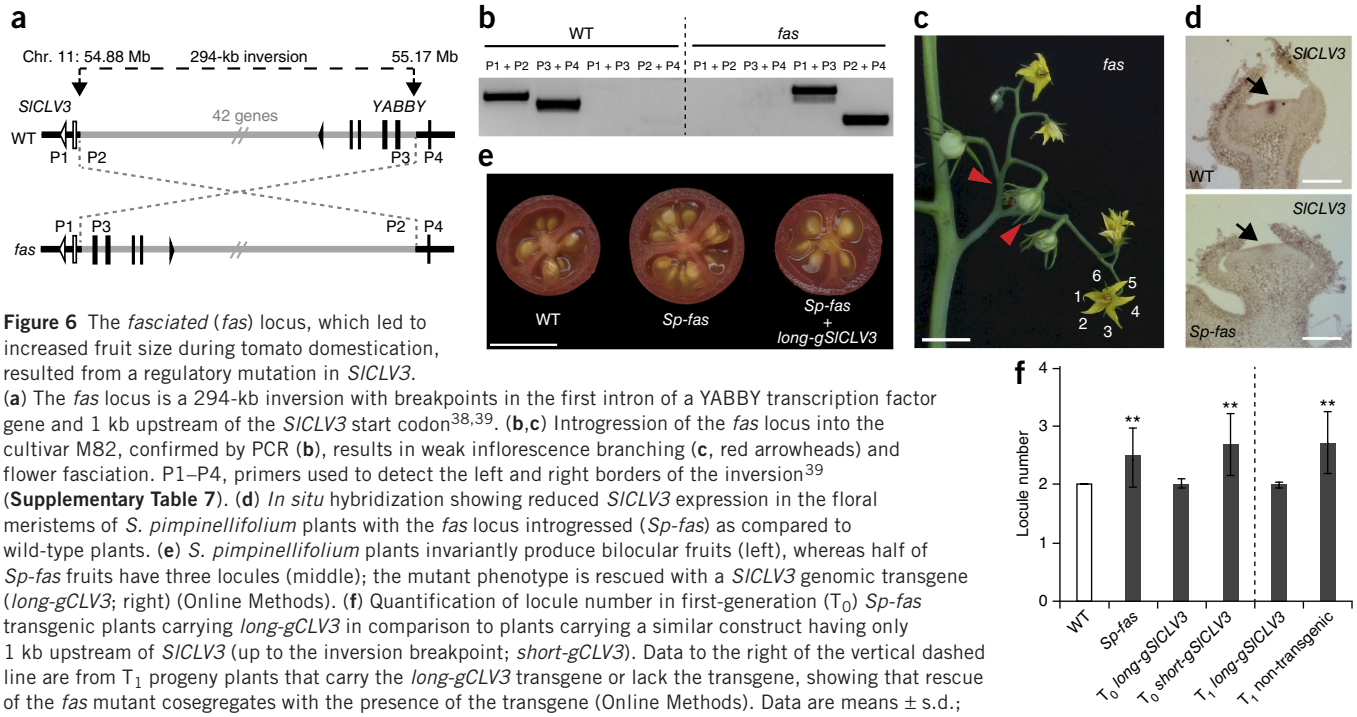

Figure 6 The *fasciated* (*fas*) locus, which led to increased fruit size during tomato domestication, resulted from a regulatory mutation in *SlCLV3*. (**a**) The *fas* locus is a 294-kb inversion with breakpoints in the first intron of a YABBY transcription factor gene and 1 kb upstream of the *SlCLV3* start codon[38,39]. (**b**,**c**) Introgression of the *fas* locus into the cultivar M82, confirmed by PCR (**b**), results in weak inflorescence branching (**c**, red arrowheads) and flower fasciation. P1–P4, primers used to detect the left and right borders of the inversion[39] (**Supplementary Table 7**). (**d**) *In situ* hybridization showing reduced *SlCLV3* expression in the floral meristems of *S. pimpinellifolium* plants with the *fas* locus introgressed (*Sp-fas*) as compared to wild-type plants. (**e**) *S. pimpinellifolium* plants invariantly produce bilocular fruits (left), whereas half of *Sp-fas* fruits have three locules (middle); the mutant phenotype is rescued with a *SlCLV3* genomic transgene (*long-gCLV3*; right) (Online Methods). (**f**) Quantification of locule number in first-generation (T_0) *Sp-fas* transgenic plants carrying *long-gCLV3* in comparison to plants carrying a similar construct having only 1 kb upstream of *SlCLV3* (up to the inversion breakpoint; *short-gCLV3*). Data to the right of the vertical dashed line are from T_1 progeny plants that carry the *long-gCLV3* transgene or lack the transgene, showing that rescue of the *fas* mutant cosegregates with the presence of the transgene (Online Methods). Data are means ± s.d.; $n \geq 200$. A two-tailed, two-sample *t* test was performed, and significant differences are represented by black asterisks: $^{**}P < 0.001$. Scale bars: 1 cm (**c**,**e**) and 100 μm (**d**).

also suffer from sterility defects (data not shown). In the context of stem cell maintenance, our data imply that addition of complete arabinose chains on CLV3 and related CLE peptides by a cascade of arabinosyltransferases is required to fully activate the conserved CLV-WUS circuit. Notably, in this respect, fasciation in *fab2* mutants is weaker than in *fin* mutants and *CR-rra3a* plants appear intermediate (**Supplementary Table 5**), suggesting that the potency of CLE peptide signaling *in planta* increases with arabinose chain length[26]. Thus, developmentally programmed or environmentally induced changes in arabinosyltransferase activity on CLV3 and related CLE peptides could be a mechanism to quantitatively control stem cell proliferation and meristem size.

Our findings show that disrupting the tomato CLV-WUS circuit has dramatic consequences for inflorescence architecture, flower production and fruit size. Increased fruit size was likely the first stage of tomato domestication, and, although many loci were involved[34], the synergistic effect of *fas* and *lc* mutations on flower and fruit fasciation may have largely been responsible for fruits that exceed 500g (refs. 35,36). In support of this idea, combining *fas* with *lc* in *S. pimpinellifolium* enhances fasciation (**Supplementary Fig. 13**). Our findings that *fas* is due to partial loss of *SlCLV3* expression and that a regulatory change in *SlWUS* is the likely cause of *lc*[16] indicate that tomato domestication relied on subtle changes in the activity of the CLV-WUS circuit. Although the CLV-WUS circuit in *Arabidopsis* seems to be buffered against large changes in *CLV3* expression[44], *fas* mutants demonstrate that even a modest decrease in expression can cause a substantial increase in fruit size, without compromising plant growth and architecture. In this respect, it is notable that our collection of *CLV* pathway mutations provided a range of fasciation, indicating that there are multiple ways to manipulate the *CLV-WUS* circuit to quantitatively control meristem size and, thus, inflorescence architecture, flower production and fruit size. We predict that the set of genes that can be targeted to achieve this control will extend to other LRR receptor–like genes and CLE genes operating in parallel and compensatory pathways[45–50] (**Fig. 3**). In this respect, the upregulation of multiple potentially functionally redundant *SlCLE* genes when *FIN* is mutated might explain the extreme fasciation in *fab* and *fin* double mutants, if higher levels of unmodified SlCLE peptides provide some activity through SlCLV1 (**Fig. 2b** and **Supplementary Fig. 3**). Notably, our results suggest that the ability to fine-tune *CLV* signaling could potentially be exploited to improve crop productivity. For example, in parallel to the improvement of tomato fruit size by *fas*, induced weak alleles of a *CLV2* homolog in maize can increase kernel row number[4], and a naturally occurring *CLV3* mutation in mustard (*Brassica rapa*) could provide increased seed production[51]. With the widespread success of the CRISPR/Cas system in plants, the entire CLV pathway, now including arabinosyltransferase genes, can be targeted in many crops to test whether customized alleles can benefit breeding.

URLs. Solanaceae Genomics Network, http://solgenomics.net/; Solanaceae Genomics Network FTP site for genomic data deposition and access, ftp://ftp.solgenomics.net/transcript_sequences/by_experiment/lippman_lab/Liberatore_etal/; tomato tissue RNA sequencing database, http://tomatolab.cshl.edu/~lippmanlab2/allexp_query.html; ImageJ software, http://rsb.info.nih.gov/ij/download.html.

METHODS

Methods and any associated references are available in the online version of the paper.

Accession codes. RNA sequencing data have been deposited to the Solanaceae Genomics Network (SGN; http://solgenomics.net/). Data are available from the following ftp link: ftp://ftp.solgenomics.net/transcript_sequences/by_experiment/lippman_lab/Liberatore_etal/.

Note: Any Supplementary Information and Source Data files are available in the online version of the paper.

ACKNOWLEDGMENTS

We thank members of the Lippman laboratory, especially S. Thomain for her initial finding of *FAB2* and for invaluable conversations that helped shape this work. We thank D. Zamir (Hebrew University of Jerusalem) for providing mutants and also Y. Eshed (Weizmann Institute of Science) for providing mutants and comments on the manuscript. We thank S. Hearn at the Cold Spring Harbor Laboratory St. Giles Advanced Microscopy Center for providing technical service for transmission electron microscopy. We thank W. Wang for assistance with tomato transformation, X. Song for advice on peptide assays, DuPont Pioneer for research support, and T. Mulligan, A. Krainer and staff from Cornell University's Long Island Horticultural Research and Extension Center in Riverhead, New York, for assistance with plant care. This research was supported by the Energy Biosciences Institute and the Fred Dickinson Chair for M.P., a National Science Foundation Graduate Research Fellowship (DGE-0914548) to K.L.L., a Gordon and Betty Moore Foundation Fellowship from the Life Sciences Research Foundation to C.A.M., grants from the National Science Foundation Plant Genome Research Program to E.v.d.K. (0922661) and to J.V.E. and Z.B.L. (1237880), and an Agriculture and Food Research Initiative competitive grant (2015-67013-22823) of the US Department of Agriculture National Institute of Food and Agriculture to Z.B.L.

AUTHOR CONTRIBUTIONS

C.X., K.L.L., C.A.M., Z.H., Y.-H.C., M.P., J.V.E., Y.M., E.v.d.K. and Z.B.L. designed and planned experiments. C.X., K.L.L., C.A.M., Z.H., Y.-H.C., C.B., M.O.-O., G.X. and Z.B.L. performed experiments and collected the data. C.X., K.L.L., C.A.M., Z.H., Y.-H.C., K.J., C.B., M.O.-O., G.X., M.P., Y.M., E.v.d.K. and Z.B.L. analyzed the data. K.L.L., C.X., Y.M., E.v.d.K. and Z.B.L. designed the research. C.X., K.L.L. and Z.B.L. wrote the manuscript.

COMPETING FINANCIAL INTERESTS

The authors declare competing financial interests: details are available in the online version of the paper.

1. Rickett, H.W. The classification of inflorescences. *Bot. Rev.* **10**, 187–231 (1944).
2. Prusinkiewicz, P., Erasmus, Y., Lane, B., Harder, L.D. & Coen, E. Evolution and development of inflorescence architectures. *Science* **316**, 1452–1456 (2007).
3. Park, S.J., Eshed, Y. & Lippman, Z.B. Meristem maturation and inflorescence architecture—lessons from the Solanaceae. *Curr. Opin. Plant Biol.* **17**, 70–77 (2014).
4. Bommert, P., Nagasawa, N.S. & Jackson, D. Quantitative variation in maize kernel row number is controlled by the *FASCIATED EAR2* locus. *Nat. Genet.* **45**, 334–337 (2013).
5. Doebley, J. The genetics of maize evolution. *Annu. Rev. Genet.* **38**, 37–59 (2004).
6. Barton, M.K. Twenty years on: the inner workings of the shoot apical meristem, a developmental dynamo. *Dev. Biol.* **341**, 95–113 (2010).
7. Clark, S.E., Williams, R.W. & Meyerowitz, E.M. The *CLAVATA1* gene encodes a putative receptor kinase that controls shoot and floral meristem size in *Arabidopsis*. *Cell* **89**, 575–585 (1997).
8. Fletcher, J.C., Brand, U., Running, M.P., Simon, R. & Meyerowitz, E.M. Signaling of cell fate decisions by CLAVATA3 in *Arabidopsis* shoot meristems. *Science* **283**, 1911–1914 (1999).
9. Ohyama, K., Shinohara, H., Ogawa-Ohnishi, M. & Matsubayashi, Y. A glycopeptide regulating stem cell fate in *Arabidopsis thaliana*. *Nat. Chem. Biol.* **5**, 578–580 (2009).
10. Stahl, Y. & Simon, R. Plant primary meristems: shared functions and regulatory mechanisms. *Curr. Opin. Plant Biol.* **13**, 53–58 (2010).
11. Schoof, H. *et al.* The stem cell population of *Arabidopsis* shoot meristems in maintained by a regulatory loop between the *CLAVATA* and *WUSCHEL* genes. *Cell* **100**, 635–644 (2000).
12. Pautler, M., Tanaka, W., Hirano, H.Y. & Jackson, D. Grass meristems I: shoot apical meristem maintenance, axillary meristem determinacy and the floral transition. *Plant Cell Physiol.* **54**, 302–312 (2013).
13. Menda, N., Semel, Y., Peled, D., Eshed, Y. & Zamir, D. *In silico* screening of a saturated mutation library of tomato. *Plant J.* **38**, 861–872 (2004).
14. Lippman, Z.B. *et al.* The making of a compound inflorescence in tomato and related nightshades. *PLoS Biol.* **6**, e288 (2008).
15. Jeong, S., Trotochaud, A.E. & Clark, S.E. The *Arabidopsis CLAVATA2* gene encodes a receptor-like protein required for the stability of the CLAVATA1 receptor-like kinase. *Plant Cell* **11**, 1925–1934 (1999).
16. Muños, S. *et al.* Increase in tomato locule number is controlled by two single-nucleotide polymorphisms located near *WUSCHEL*. *Plant Physiol.* **156**, 2244–2254 (2011).
17. Reinhardt, D., Frenz, M., Mandel, T. & Kuhlemeier, C. Microsurgical and laser ablation analysis of interactions between the zones and layers of the tomato shoot apical meristem. *Development* **130**, 4073–4083 (2003).
18. Zhang, Y., Yang, S., Song, Y. & Wang, J. Genome-wide characterization, expression and functional analysis of *CLV3/ESR* gene family in tomato. *BMC Genomics* **15**, 827 (2014).
19. Diévart, A. *et al. CLAVATA1* dominant-negative alleles reveal functional overlap between multiple receptor kinases that regulate meristem and organ development. *Plant Cell* **15**, 1198–1211 (2003).
20. Ogawa-Ohnishi, M., Matsushita, W. & Matsubayashi, Y. Identification of three hydroxyproline O-arabinosyltransferases in *Arabidopsis thaliana*. *Nat. Chem. Biol.* **9**, 726–730 (2013).
21. Kieliszewski, M.J. & Lamport, D.T. Extensin: repetitive motifs, functional sites, post-translational codes, and phylogeny. *Plant J.* **5**, 157–172 (1994).
22. Lamport, D.T., Kieliszewski, M.J., Chen, Y. & Cannon, M.C. Role of the extensin superfamily in primary cell wall architecture. *Plant Physiol.* **156**, 11–19 (2011).
23. Cannon, M.C. *et al.* Self-assembly of the plant cell wall requires an extensin scaffold. *Proc. Natl. Acad. Sci. USA* **105**, 2226–2231 (2008).
24. Matsubayashi, Y. Small post-translationally modified peptide signals in. *Arabidopsis. Arabidopsis Book* **9**, e0150 (2011).
25. Xu, T.T., Song, X.F., Ren, S.C. & Liu, C.M. The sequence flanking the N-terminus of the CLV3 peptide is critical for its cleavage and activity in stem cell regulation in *Arabidopsis*. *BMC Plant Biol.* **13**, 225 (2013).
26. Shinohara, H. & Matsubayashi, Y. Chemical synthesis of *Arabidopsis* CLV3 glycopeptide reveals the impact of hydroxyproline arabinosylation on peptide conformation and activity. *Plant Cell Physiol.* **54**, 369–374 (2013).
27. Doudna, J.A. & Charpentier, E. Genome editing. The new frontier of genome engineering with CRISPR-Cas9. *Science* **346**, 1258096 (2014).
28. Belhaj, K., Chaparro-Garcia, A., Kamoun, S., Patron, N.J. & Nekrasov, V. Editing plant genomes with CRISPR/Cas9. *Curr. Opin. Biotechnol.* **32**, 76–84 (2015).
29. Brooks, C., Nekrasov, V., Lippman, Z.B. & Van Eck, J. Efficient gene editing in tomato in the first generation using the clustered regularly interspaced short palindromic repeats/CRISPR-associated9 system. *Plant Physiol.* **166**, 1292–1297 (2014).
30. Nimchuk, Z.L., Tarr, P.T. & Meyerowitz, E.M. An evolutionarily conserved pseudokinase mediates stem cell production in plants. *Plant Cell* **23**, 851–854 (2011).
31. Gille, S., Hansel, U., Ziemann, M. & Pauly, M. Identification of plant cell wall mutants by means of a forward chemical genetic approach using hydrolases. *Proc. Natl. Acad. Sci. USA* **106**, 14699–14704 (2009).
32. Velasquez, S.M. *et al.* O-glycosylated cell wall proteins are essential in root hair growth. *Science* **332**, 1401–1403 (2011).
33. Egelund, J. *et al.* Molecular characterization of two *Arabidopsis thaliana* glycosyltransferase mutants, *rra1* and *rra2*, which have a reduced residual arabinose content in a polymer tightly associated with the cellulosic wall residue. *Plant Mol. Biol.* **64**, 439–451 (2007).
34. Tanksley, S.D. The genetic, developmental, and molecular bases of fruit size and shape variation in tomato. *Plant Cell* **16** (suppl.), S181–S189 (2004).
35. Barrero, L.S. & Tanksley, S.D. Evaluating the genetic basis of multiple-locule fruit in a broad cross section of tomato cultivars. *Theor. Appl. Genet.* **109**, 669–679 (2004).
36. Lippman, Z. & Tanksley, S.D. Dissecting the genetic pathway to extreme fruit size in tomato using a cross between the small-fruited wild species *Lycopersicon pimpinellifolium* and *L. esculentum* var. Giant Heirloom. *Genetics* **158**, 413–422 (2001).
37. van der Knaap, E. *et al.* What lies beyond the eye: the molecular mechanisms regulating tomato fruit weight and shape. *Front. Plant Sci.* **5**, 227 (2014).
38. Cong, B., Barrero, L.S. & Tanksley, S.D. Regulatory change in YABBY-like transcription factor led to evolution of extreme fruit size during tomato domestication. *Nat. Genet.* **40**, 800–804 (2008).
39. Huang, Z. & van der Knaap, E. Tomato *fruit weight 11.3* maps close to *fasciated* on the bottom of chromosome 11. *Theor. Appl. Genet.* **123**, 465–474 (2011).
40. Lombard, V., Golaconda Ramulu, H., Drula, E., Coutinho, P.M. & Henrissat, B. The carbohydrate-active enzymes database (CAZy) in 2013. *Nucleic Acids Res.* **42**, D490–D495 (2014).
41. Yin, Y., Mohhen, D., Gelineo-Albersheim, I., Xu, Y. & Hahn, M. in *Annual Plant Reviews: Plant Polysaccharides: Biosynthesis and Bioengineering* (ed. Ulvskov, P.) (Wiley-Black, 2011).
42. Petersen, B.L., Faber, K. & Ulvskov, P. in *Annual Plant Reviews: Plant Polysaccharides: Biosynthesis and Bioengineering* (ed. Ulvskov, P.) (Wiley-Black, 2011).
43. Schnabel, E.L. *et al.* The *ROOT DETERMINED NODULATION1* gene regulates nodule number in roots of *Medicago truncatula* and defines a highly conserved, uncharacterized plant gene family. *Plant Physiol.* **157**, 328–340 (2011).
44. Müller, R., Borghi, L., Kwiatkowska, D., Laufs, P. & Simon, R. Dynamic and compensatory responses of *Arabidopsis* shoot and floral meristems to CLV3 signaling. *Plant Cell* **18**, 1188–1198 (2006).
45. Betsuyaku, S. *et al.* Mitogen-activated protein kinase regulated by the CLAVATA receptors contributes to shoot apical meristem homeostasis. *Plant Cell Physiol.* **52**, 14–29 (2011).

46. DeYoung, B.J. *et al*. The CLAVATA1-related BAM1, BAM2 and BAM3 receptor kinase-like proteins are required for meristem function in. *Arabidopsis. Plant J.* **45**, 1–16 (2006).
47. DeYoung, B.J. & Clark, S.E. BAM receptors regulate stem cell specification and organ development through complex interactions with CLAVATA signaling. *Genetics* **180**, 895–904 (2008).
48. Kinoshita, A. *et al*. RPK2 is an essential receptor-like kinase that transmits the CLV3 signal in *Arabidopsis*. *Development* **137**, 3911–3920 (2010).
49. Müller, R., Bleckmann, A. & Simon, R. The receptor kinase CORYNE of *Arabidopsis* transmits the stem cell–limiting signal CLAVATA3 independently of CLAVATA1. *Plant Cell* **20**, 934–946 (2008).
50. Nimchuk, Z.L., Zhou, Y., Tarr, P.T., Petersen, B.A. & Meyerowitz, E.M. Plant stem cell maintenance by transcriptional cross-regulation of related receptor kinases. *Development* **142**, 1043–1049 (2015).
51. Fan, C. *et al*. A novel single-nucleotide mutation in a *CLAVATA3* gene homolog controls a multilocular silique trait in *Brassica rapa* L. *Mol. Plant* **7**, 1788–1792 (2014).

ONLINE METHODS

Plant materials and growth conditions. Six branched and fasciated inflorescence mutants forming two complementation groups were isolated from a saturated mutagenesis population in the standard genetic background cultivar M82 (ref. 13). One complementation group, comprising a single EMS mutant, *e0497*, was designated *fasciated and branched* (*fab*). The other five mutants (three EMS and two FN alleles: *fin-e4489*, *fin-e4643*, *fin-e9501*, *fin-n2326* and *fin-n5644*) were designated *fasciated inflorescence* (*fin*). We rescreened the mutagenesis population and, using the same EMS mutagenesis protocol, developed and screened a new population of 3,000 M_2 families. We identified two alleles of a new mutant phenotypically similar but not complementary to *fab* that was designated *fab2* (*fab2-e4891* and *fab2-e0051*). Three reference alleles, *fab-e0497*, *fin-e4489* and *fab2-e4891*, were backcrossed to the M82 parental line at least three times before generating F_2 mapping populations or double mutants. F_2 mapping populations were generated by crossing reference alleles to *S. pimpinellifolium* and self-fertilizing the F_1 plants. *fas* was backcrossed to M82 six times and to *S. pimpinellifolium* ten times, using PCR genotyping markers that identify the left and right breakpoints of the inversion[39]. *lc* was also backcrossed to *S. pimpinellifolium* ten times. All double mutants were generated using standard crossing schemes and were confirmed by genotyping. Seeds used for meristem measurements, RNA sequencing and RNA *in situ* hybridization were pregerminated in petri dishes on Whatman paper moistened with sterile water. Seedlings with similar germination staging were transferred to soil in 72-cell plastic flats and grown in the greenhouse. Seeds used for transient expression were directly sown and germinated in soil in 72-cell plastic flats and grown in the greenhouse. Greenhouse plants were grown under natural light with supplementation from high-pressure sodium bulbs (50 mM/m^2/s) on a 16-h light/8-h dark photoperiod. Daytime and nighttime temperatures were 26–28 °C and 18–20 °C, respectively.

CRIPSR/Cas9 gene editing and genotyping, and phenotyping of the resulting mutants. CRISPR/Cas9 mutagenesis, plant regeneration and greenhouse care were performed as described[29]. Briefly, constructs were designed to produce defined deletions within each target gene-coding sequence using two sgRNAs alongside the *Cas9* endonuclease gene (see **Supplementary Table 6** for a list of the sgRNAs used in this study). For genotyping of each first-generation (T_0) transgenic line, three different leaf samples were collected to capture all possible induced mutant alleles due to sectoring (chimerism), and genomic DNA was extracted using a standard cetrimonium bromide (CTAB) protocol. Each plant was genotyped by PCR for the presence of the *Cas9*-sgRNA1-sgRNA2 construct with primers designed to amplify a region spanning the 3′ end of the *35S* promoter and the 5′ end of *Cas9*. The CRISPR/Cas9 T-DNA–positive lines were further genotyped for indel mutations using a forward primer to the left of sgRNA1 and a reverse primer to the right of sgRNA2 (**Supplementary Table 6**). PCR products from selected plants were purified for cloning into the pSC-A-amp/kan vector (Stratagene). A minimum of eight clones per PCR product were sequenced. Homozygosity for the desired deletion occurred but was rare. We typically obtained biallelic or chimeric plants in which indels occurred at one or both sgRNA target sites. Only plants in which all sequenced alleles were mutated were phenotyped, to ensure that quantification and comparison of fasciation were based on effectively null mutants. For quantification of the floral organs of the genotyped mutants, we randomly collected about 4 flowers from each mutant and counted floral organs; we then pooled the data from 3–5 different mutants to compare with the floral organs of wild-type plants grown under the same condition.

Meristem imaging. Stereomicroscope imaging of meristems was performed as described previously[52]. Briefly, hand-dissected tomato meristems were captured on a Nikon SMZ1500 microscope. For SEM, meristems were dissected by hand and passed through a dehydrating ethanol series, dried using a critical-point dryer (Tousimis), coated in gold particles and imaged under a Hitachi S-3500N microscope.

Transmission electron microscopy. Tomato vegetative meristems from 9-d-old seedlings were fixed in 2% glutaraldehyde and 2% paraformaldehyde in 0.1 M PBS overnight and then post-fixed in 1% osmium tetroxide in 1.5% potassium ferrocyanide. Samples were dehydrated in a graded alcohol series followed by 100% dry acetone. Samples were infiltrated with agitation in 50% Epon Araldite resin in 100% acetone for 2 h and then overnight in 100% resin. Samples were flat embedded in resin in BEEM capsules from which the conical ends had been removed and were capped with the flat lid of the capsule. Plastic blocks were carefully trimmed and positioned for sectioning to obtain longitudinal sections through the meristem region. Thin sections were collected on Butvar-coated 1 × 2 mm nickel slot grids (Veco, Electron Microscopy Sciences) and counterstained in lead citrate stain. Samples were examined with a Hitachi H700 transmission electron microscope at 75 kV and were recorded on Kodak 4489 film that was then scanned at 2,400 dpi using an Epson Perfection V750 Pro scanner.

Meristem transcriptome profiling. Vegetative meristem collection, RNA extraction and library preparation for wild-type, *fin* and *fab* plants were performed as described[52]. Briefly, total RNA was extracted from 30–50 meristems per biological replicate using a PicoPure RNA Extraction kit (Arcturus). mRNA was purified from 1–5 µg of total RNA for library construction using the ScriptSeq v2 RNA library preparation kit (Epicentre) with barcodes. The quantity and size distribution of each individual RNA sequencing library were detected on a Bioanalyzer 2100 (Agilent Technologies). Two biological replicates per genotype were generated. Five barcoded libraries were pooled with relatively equal concentrations (determined by qRT-PCR quantification) for one lane of Illumina paired-end 100-bp sequencing on an Illumina HiSeq sequencing machine. See methods of data analysis in the **Supplementary Note**.

Tissue-specific expression patterns for *SlCLV3*, *SlCLE3*, *SlCLE9*, *FAB*, *FIN*, *FAB2* and *SlRRA3a* were obtained from the tomato tissue RNA sequencing database. RNA sequencing data from different tissues (for example, in **Fig. 2f,g**) were mined from the tomato genome project transcriptome profiling data sets deposited in the Sequence Read Archive (SRA) under accession SRP010775 (ref. 53) and from our meristem maturation atlas[52].

***In situ* hybridization.** RNA *in situ* hybridization was performed using standard protocols[54], with slight modifications. Briefly, full-length coding sequences for tomato *SlWUS* (*Solyc02g083950*), *SlCLV3* (*Solyc11g071380*) and *FAB* (*Solyc04g081590*) were amplified from M82 cDNA using Phusion Taq (Invitrogen), and the resulting products were ligated into the StrataClone pSC-A-amp/kan vector (Agilent Technologies). Plasmids were linearized and, depending on the orientation of the gene insert, T7 or T3 RNA polymerase was used for *in vitro* transcription. Full-length probes were used for hybridization. SAM stages were defined as described previously[52]. For fixation, meristems were dissected by hand and fixed in 4% paraformaldehyde with 0.3% Triton X-100 under vacuum for 20 min at 400 mm Hg.

Map-based cloning. Markers for recombinant mapping and genotyping were generated using SNPs and indels identified in comparison of *Solanum lycopersicum* and *S. pimpinellifolium*[53]. By using 76 F_2 mutants and molecular markers derived from the *S. pimpinellifolium* genome sequence, we mapped the locus for *fab-e0497* to a 325-kb interval containing 45 genes on the bottom of chromosome 4, including *Solyc04g081590*, the closest homolog of *CLV1*. Using a similar approach with 624 F_2 mutants, we mapped the locus for the *fin-e4489* mutant to a 1-Mb region in the middle of chromosome 11 containing 71 genes. As a lack of recombination prevented further fine mapping, meristem-enriched mRNA was extracted from *fin-e4489* for deep cDNA sequencing (mRNA-seq). A total of 42 million paired-end 100-bp Illumina sequencing reads were aligned to the 1-Mb interval, and a single nonsense mutation was detected in *Solyc11g064850*. Sanger sequencing of *fin*-e4632 identified a missense mutation in the same gene. The other *fin* alleles (*fin-n2326*, *fin-e9501* and *fin-n5644*) could not be amplified by PCR, indicating that there were large deletions encompassing the *Solyc11g064850* gene location, which was confirmed by RT-PCR. Using 42 F_2 mutants, we mapped the locus for the *fab2-e4981* mutant to a 100-kb region on the bottom of chromosome 8 containing 7 genes. Sanger sequencing identified a missense mutation in *Solyc08g075340*. Sequencing of the second allele of *fab2*, *fab2-e0051*, identified a nonsense mutation in *Solyc08g075340*.

Transient expression in tomato protoplasts. To generate the transient expression constructs for analysis of subcellular localization, eGFP was fused to the C termini of FIN, FAB2 and SlRRA3a. To produce a series of Golgi markers, mCherry was fused to the C termini of Man49 (*Arabidopsis* α-1,2 mannosidase I-49)[55], MUR3 (*Arabidopsis* β-1,2-galactosyltransferase)[56] and ST (*Rattus norvegicus* α-2,6-sialyltransferase)[57] to create *cis*-, *medial*- and *trans*-Golgi markers, respectively. Fusion protein expression was driven by the cauliflower mosaic virus (CaMV) *35S* promoter in transient expression vectors, as described previously[58]. The transient expression protocol was modified from the *Arabidopsis* mesophyll protoplast system[59]. Well-expanded leaves from 10- to 14-d-old tomato plants were cut into 0.5- to 1-mm leaf strips and digested with enzyme solution (1.5% cellulase R10 (Yakult Honsha), 0.4% macerozyme (Yakult Honsha), 20 mM MES (pH 5.7), 0.4 M mannitol, 20 mM KCl, 10 mM $CaCl_2$ and 0.1% BSA) in a 90-mm Petri dish for 4 h in the dark with gentle shaking at 40–50 rpm. The digestion products were filtered using 75-μm nylon mesh (Fisher) in a 50-ml Falcon tube. Cells were collected by centrifugation at 100*g* for 2 min. The cells were washed by resuspending them in precooled W5 solution (2 mM MES, pH 5.7, 125 mM $CaCl_2$, 154 mM NaCl, 0.1 M glucose and 5 mM KCl), and cells were finally resuspended in MMG solution (4 mM MES, pH 5.7, 0.5 M mannitol and 15 mM $MgCl_2$) to a concentration at 2×10^5 cells/ml for immediate transfection. For transfection, 5–10 μg of plasmid of 5–10 kb in size was added to 100 μl of protoplast cell suspension in a 2-ml microfuge tube, and samples were then gently mixed well with an equal volume of PEG solution (40% PEG in 0.2 M mannitol and 100 mM $CaCl_2$). The transfection mixtures were incubated at room temperature for 10 min, and cells were then washed with W5 solution. Cells were resuspended in W5 solution and incubated at 28 °C for 12 h before collection for microscopy or other experiments. Imaging was performed on a Zeiss Axioplan 2 fluorescence microscope with an AxioCam camera.

Monosaccharide analysis of the cell wall. Preparation and analysis of cell wall material (alcohol-insoluble residue, or AIR) was performed as described[60]. Neutral sugars and uronic acids from non-cellulosic polysaccharides in AIR were released by hydrolysis with trifluoroacetic acid (TFA). Approximately 1 mg of AIR was hydrolyzed with 250 μl of 2 M TFA at 121 °C for 90 min. The TFA-soluble material was split into two equal parts, one for uronic acid determination and one for neutral sugar determination. Uronic acid content was determined by subjecting the hydrolyzate to a CarboPac PA200 anion-exchange column with an ICS-3000 Dionex chromatography system. The elution profile consisted of a linear gradient of 50–200 mM sodium acetate in 0.1 M NaOH in 10 min at 0.4 ml/min. Neutral sugar composition was determined by derivatization with alditol acetate as described[61]. In brief, monosaccharides in the hydrolyzate were reduced with $NaBH_4$ (20 mg/ml dissolved in 1 M NH_4OH) at room temperature for 1 h and then peracetylated with acetic anhydride and pyridine at 121 °C for 20 min. The alditol acetates generated were separated on a gas chromatograph equipped with a Supelco SP2380 column (Sigma-Aldrich) and analyzed by a flame ionization detector (FID) (Agilent Technologies, 7890A).

Sequential extraction of cell wall polymers. Cell wall polymers were sequentially extracted as described previously[31]. Freeze-dried plant materials were ground to fine powder. About 5 mg of ground material was extracted overnight in 50 mM ammonium formate buffer, pH 4.5, at 37 °C with shaking at 200 rpm. After incubation, the samples were centrifuged for 10 min at 20,800*g*, and the supernatant was collected. The remaining pellet was washed three times with 1 ml of water per wash and centrifuged, and the resulting supernatants were pooled with the supernatant from the first spin. The supernatant was precipitated overnight in 80% ethanol and centrifuged for 10 min at 20,800*g*. The precipitated fraction was freeze dried, representing the buffer extract. The buffer-insoluble pellet was digested with 0.02 U pectin methylesterase (EC3.1.1.11, Novozymes) and endopolygalacturonanase M2 (EC3.2.1.15, Megazyme) in 1 ml of 50 mM ammonium formate buffer (pH 4.5) overnight at 37 °C. After digestion, the samples were treated for 10 min at 99 °C and centrifuged for 10 min at 20,800*g*, and the supernatant was collected as the EPG/PME fraction (pectin extract). The remaining pellet was digested with 10 U endoglucanase II (EGII, Megazyme) in 1 ml of 50 mM ammonium formate buffer (pH 4.5) overnight at 37 °C, heat inactivated for 10 min at 99 °C and centrifuged for 10 min at 20,800*g*; the supernatant was collected as a hemicellulosic/cellulosic extract. The remaining pellet was treated with 1 ml of saturated $Ba(OH)_2$ (~0.22 M) solution for 6 h at 105 °C. The pellet resulting from centrifugation was washed three times with 1 ml of water per wash and centrifuged. The resulting supernatants (extensin fraction) were pooled and neutralized with 1 M sulfuric acid, and the precipitating salts were removed by centrifugation. The remaining pellet (residue) and all fractions were freeze dried and analyzed for monosaccharide composition as described above.

***In planta* peptide treatment of tomato apices.** Peptide treatment of tomato apical meristems was modified from previous methods[26,62]. Sterilized tomato seeds were distributed onto two layers of Whatman paper moistened with sterile water in a 180-mm petri dish. The seeds were pregerminated at 28 °C for 1–2 d. Seeds with similar staging were selected for further growth in a 50-ml Falcon tube (10 seeds/tube) with 10 ml of liquid medium containing half-strength Murashige and Skoog salt mixture (Sigma-Aldrich), 1% sucrose and 0.5 g/l MES (pH 5.8) and supplemented with different concentrations of peptides. The Falcon tubes were incubated on a roller bank with a 16-h light/8-h dark photoperiod at 28 °C for 10 d. Chemical synthesis of arabinosylated SlCLE peptides was performed as described previously[26].

Tomato shoot apical meristem imaging and size measurement of treated meristems. After peptide treatment, SAMs were cleared for imaging and size quantification. Individual SAMs from each treatment were dissected and fixed in FAA (1% formaldehyde, 0.5% acetic acid and 50% ethanol) overnight at 4°C. The fixed SAMs were sequentially washed with 70%, 85% and 100% ethanol for 30 min each wash and dehydrated for 60 min in 100% ethanol; they were then immersed in an ethanol:methyl salicylate solution (1:1) for an additional 60 min. Fixed tissue was transferred to methyl salycilate (100%) for storage before microscopy. Slides were sealed with Vaseline to keep the SAMs immersed in methyl salicylate. Imaging by Normarsky illumination was conducted using a Leica DMRB microscope (Leica Microsystems). Micrographs were acquired with a Leica MicroPublisher 5.0 RTV digital camera system using Q-IMAGING software. All images were taken at the focal plane corresponding to the median optical section of the SAM. The size of each SAM was determined by outlining and calculating the meristem area between the basal edges of two opposite leaf primordia using 'freehand selections' and 'measure', respectively, in ImageJ software. The peptide treatment assays were performed three times with similar results.

Quantitative RT-PCR. qRT-PCR was performed as described previously[52]. Briefly, total RNA from vegetative meristems and shoot apices was extracted with the PicoPure RNA Extraction kit and the RNeasy mini kit (Qiagen), respectively. One microgram of total RNA was treated with DNase I and used for cDNA synthesis with a SuperScript III reverse-transcriptase kit (Invitrogen). qRT-PCR was performed using gene-specific primers in the iQ SYBR Green SuperMix (Bio-Rad) reaction system on the CFX96 Real-Time system (Bio-Rad), following the manufacturer's instructions (**Supplementary Table 7**). The tomato *UBIQUITIN* gene was used as an internal control.

Constructs for transformation and complementation of *Sp-fas*. The binary vector (pHaoNM) used in transgenic complementation of *Sp-fas* was modified from the standard vector pCAMBIA1300. The two constructs used for complementation tests were generated through the following steps. First, fosmid SL_FOS0151E08 from tomato accession Heinz 1706 was digested at MfeI and SacI sites to obtain a 4,320-bp fragment containing the *SlCLV3* gene. This fragment was then ligated into pHaoNM at the EcoRI and SacI sites (pHC1). A 5,233-bp fragment upstream of the *SlCLV3* gene was isolated from SL_FOS0151E08 by digesting at SacI and NsiI sites. This fragment was ligated into pHC1 at the SacI and SbfI sites to create the complementation construct named *long-gCLV3*, containing the *SlCLV3* gene with 5,465 bp upstream of the start codon and 3,445 bp downstream of the stop codon. For the control construct *short-gCLV3*, a PCR product was amplified with primers 12EP315 and 12EP389 (**Supplementary Table 7**). The PCR product was then digested with SacI and PstI and inserted into pHC1at the SacI and SbfI sites. The resulting

doi:10.1038/ng.3309

short-gCLV3 construct contained the *SlCLV3* gene, 1,008 bp upstream of the start codon of *SlCLV3* (up to the *fas* inversion breakpoint) and 3,445 bp downstream of the stop codon.

To test whether *SlCLV3* was responsible for the *fas* phenotype, *long-gCLV3* and *short-gCLV3* were introduced separately into *Sp-fas* using *Agrobacterium*-mediated transformation (*Agrobacterium tumefaciens* strain LBA4404). We generated 18 first-generation (T_0) transgenic plants, which all carried 1 or 2 insertions of *long-gCLV3*. All 18 plants were used for phenotypic analysis of fruit locule number (n 200). We also generated 18 T_0 plants carrying *short-gCLV3*, and we phenotyped 16 plants that carried 1 or 2 insertions. Two plants that were found by Southern blot to carry four and six copies of the transgene showed evidence of cosuppression and were therefore excluded from analysis. A more detailed analysis of complementation of *fas* with *long-gCLV3* was performed in T_1 progeny plants derived from a T_0 plant with a single transgene insertion. Rescue of bilocular fruit cosegregated with the presence of the *long-gCLV3* transgene, whereas *short-gCLV3* had no effect (**Fig. 6**). Genotyping for the presence of the transgene in T_1 progeny plants was performed using PCR primers that amplified a fragment of the pCAMBIA1300 backbone.

52. Park, S.J., Jiang, K., Schatz, M.C. & Lippman, Z.B. Rate of meristem maturation determines inflorescence architecture in tomato. *Proc. Natl. Acad. Sci. USA* **109**, 639–644 (2012).
53. Tomato Genome Consortium. The tomato genome sequence provides insights into fleshy fruit evolution. *Nature* **485**, 635–641 (2012).
54. Jackson, D.P. in *Molecular Plant Pathology: A Practical Approach* (eds. Gurr, S.J., Bowles, D.J. & McPherson, M.J.) 163–174 (Oxford University Press, 1992).
55. Saint-Jore-Dupas, C. *et al.* Plant N-glycan processing enzymes employ different targeting mechanisms for their spatial arrangement along the secretory pathway. *Plant Cell* **18**, 3182–3200 (2006).
56. Chevalier, L. *et al.* Subcompartment localization of the side chain xyloglucan-synthesizing enzymes within Golgi stacks of tobacco suspension-cultured cells. *Plant J.* **64**, 977–989 (2010).
57. Nelson, B.K., Cai, X. & Nebenfuhr, A. A multicolored set of *in vivo* organelle markers for co-localization studies in *Arabidopsis* and other plants. *Plant J.* **51**, 1126–1136 (2007).
58. Xu, C. *et al.* Degradation of MONOCULM 1 by APC/C^{TAD1} regulates rice tillering. *Nat. Commun.* **3**, 750 (2012).
59. Yoo, S.D., Cho, Y.H. & Sheen, J. *Arabidopsis* mesophyll protoplasts: a versatile cell system for transient gene expression analysis. *Nat. Protoc.* **2**, 1565–1572 (2007).
60. Xiong, G., Cheng, K. & Pauly, M. Xylan O-acetylation impacts xylem development and enzymatic recalcitrance as indicated by the *Arabidopsis* mutant *tbl29*. *Mol. Plant* **6**, 1373–1375 (2013).
61. York, W.S., Darvill, A.G., McNeil, M. & Albersheim, P. 3-deoxy-D-manno-2-octulosonic acid (KDO) is a component of rhamnogalacturonan II, a pectic polysaccharide in the primary cell walls of plants. *Carbohydr. Res.* **138**, 109–126 (1985).
62. Fiers, M. *et al.* The CLAVATA3/ESR motif of CLAVATA3 is functionally independent from the nonconserved flanking sequences. *Plant Physiol.* **141**, 1284–1292 (2006).